A Journal of the Gesellschaft Deutscher Chemiker

Angewandte Chemie

GDCh

International Edition

www.angewandte.org

Accepted Article

Title: Rational Design of Two-photon Fluorogenic Probe for Visualizing Monoamine Oxidase A Activity in Human Glioma Tissues

Authors: Haixiao Fang, Hang Zhang, Lin Li, Yun Ni, Riri Shi, Zheng Li, Xuekang Yang, Bo Ma, Chengwu Zhang, Qiong Wu, Changmin Yu, Naidi Yang, Shao Q. Yao, and Wei Huang

To be cited as: *Angew. Chem. Int. Ed.* 10.1002/anie.202000059
Angew. Chem. 10.1002/ange.202000059

Link to VoR: http://dx.doi.org/10.1002/anie.202000059
http://dx.doi.org/10.1002/ange.202000059

WILEY-VCH

10.1002/anie.202000059

COMMUNICATION

WILEY-VCH

Rational Design of Two-photon Fluorogenic Probe for Visualizing Monoamine Oxidase A Activity in Human Glioma Tissues

Haixiao Fang, Hang Zhang, Lin Li, Yun Ni, Riri Shi, Zheng Li, Xuekang Yang, Bo Ma, Chengwu Zhang, Qiong Wu, Changmin Yu, Naidi Yang, Shao Q. Yao* and Wei Huang**

Abstract: *Monoamine oxidases have two functionally distinct but structurally similar isoforms (MAO-A and -B). The ability to differentiate them by using fluorescence detection/imaging technology is of significant biological relevance, but highly challenging with available chemical tools. Herein, we report the first MAO-A-specific two-photon fluorogenic probe (**F1**), capable of selective imaging of endogenous MAO-A enzymatic activities from a variety of biological samples, including MAO-A expressing neuronal SY-SY5Y cells, the brain of tumor-bearing mice and human Glioma tissues by using two-photon fluorescence microscopy (TPFM) with minimal cytotoxicity.*

Monoamine oxidases (MAOs) are important mammalian enzymes that catalyze the transformation of various neurotransmitters including serotonin, dopamine, phenethylamine, and others.[1] They are normally expressed on the outer membrane of mitochondria in cells. In human, MAOs have been found to play key roles in maintaining the homeostasis of neurotransmission. At present, there are two known human MAOs (i.e. MAO-A and MAO-B), which, despite high sequence homology (~70%), differ significantly in their biological roles, cell distributions and substrate specificity.[2] Abnormal MAO-A and -B activities are closely related to several mental illnesses and neurodegenerative diseases.[3] For example, studies have found that high expression of MAO-A is closely associated with schizophrenia and depression, while MAO-B is abundantly expressed in the brain of patients with Parkinson's disease (PD) and Alzheimer's disease (AD).[4,5] MAO-A has a strong affinity for serotonin and norepinephrine, and MAO-B mainly metabolizes benzylamine and phenethylamine.

Due to the therapeutic potential of human MAOs, chemical tools capable of selectively interogating these enzymes have been actively pursued for years.[6] Amongst the best-known small-molecule MAO inhibitors, clorgyline (**CL**) confers good selectivity against MAO-A, while known MAO-B selective inhibitors include pargyline (**PA**), selegiline, and rasagiline.[6] Some of these compounds are already being used in the treatment of various neurodegerative diseases.[6c] On the other hand, in order to selectively detect individual MAO enzymatic activities from cells and tissues, researchers have turned to the development of small-molecule fluorogenic probes (SMFPs);[6c,7] of special note, two-photon fluorogenic probes (TPFPs) when combined with advanced two-photon fluorescence microscopy (TPFM) are able to penetrate tissues deeper and provoke less optical damage at a higher resolution than one-photon fluorogenic probes (OPFPs).[8] Up to date, MAO TPFPs have been mainly designed to detect either MAO-B or both isoforms of MAOs.[9] For MAO-A-specific detection, however, only OPFPs have been reported thus far, including three reaction- and one binding-based probes (Figure 1A).[10] Ma and co-workers first reported a novel MAO-A specific OPFP (**^{AC}probe**) for visualizing MAO-A activity in live cells based on a substrate-oxidized enzymatic reaction.[10a] The same group subsequently disclosed a MAO-A-specific OPFP (**^{Angew}probe**) by covalently linking resorufin to the MAO-A-specific inhibitor **CL**.[10b] Furthermore, Li and colleagues constructed an "enzyme-recognition moiety" within a NIR-fluorophore to obtain a MAO-A-specific OPFP (**^{CC}probe**) suitable for *in vivo* imaging.[10c] Zhu and co-workers used another strategy by designing an environmentally sensitive MAO-A specific OPFP, the first fluorogenic, non-covalent "inhibitor-like" probe for MAO-A detection.[10d] Notwithstanding, specific TPFPs capable of imaging MAO-A activities directly from live mammalian cells and deep tissues with minimal MAO-B cross-reactivity have yet to be elucidated.

We previously reported the first MAO-B specific TPFP (i.e. **U1** in Figure 1B), which was successfully used to image MAO-B-specific activities from live PD models.[9a] **U1** contains a MAO-reactive propylamine warhead (WH) and a two-photon fluorescence reporter, 2-methylamino-6-acetylnaphthanlene (acedan, or "fluorophore"). Upon further inspection of molecular docking results of **U1** bound to MAO-A and -B, respectively, we found the probe interacted with each enzyme's active site differently (Figure 1B, right); while **U1** approached MAO-B and projected its amine group close to the enzyme's active-site-bound FAD (a cofactor for both MAO-A and -B[6]) as previously reported,[9a] the acetyl group from its acedan moiety in the **U1**/MAO-A complex was shown to point towards FAD instead. Anticipating that the oxidation ability of FAD in MAO-A/-B towards their respective substrates would be roughly equivalent,[11] we endeavored to redesign **U1** with the aim of achieving a MAO-A specific TPFP (Figure 1C/D); we first retained the structure of the naphthalene in **U1** by exchanging the position of "WH" and "fluorophore", followed by combining the resulting structure with *N*-alkylated tetrahydropyridine to obtain **F1**, as shown in Figure 1 (in blue halo). The use of tetrahydropyridine as the new WH design in **F1** was based on the well-established tetrahydropyridine/pyridinium (e.g. MPTP/MPP$^+$) conversion properties catalyzed by MAO-B.[12] Subsequent docking results of **F1** with various crystallographic structures of MAO-A/-B (Table S1) confirmed what was earlier predicted (Figure 1B, right bottom, and Figure S1); in sharp contrast to **U1**/MAO-A structure, the *N*-alkylated tetrahydropyridine in the docked **F1**/MAO-A complex was shown

[*] H. X. Fang, H. Zhang, Y. Ni, R. R. Shi, Z. Li, Dr. C. W. Zhang, Dr. Q. Wu, Dr. C. M. Yu, Dr. N. D. Yang, Prof. Dr. L. Li, Prof. Dr. W. Huang
Key Laboratory of Flexible Electronics (KLOFE) & Institute of Advanced Materials (IAM), Nanjing Tech University (NanjingTech) 30 South Puzhu Road, Nanjing, 211816, P. R. China.
E-mail: iamlli@njtech.edu.cn
Dr. X. Yang
Department of Burns and Cutaneous Surgery, Xijing Hospital, The Fourth Military Medical University, Xi'an, 710032, P.R. China
Dr. B. Ma
School of Pharmaceutical Sciences, Nanjing Tech University, Nanjing 210023, P. R. China
Prof. Dr. S. Q. Yao
Department of Chemistry, National University of Singapore, 3 Science Drive 3, 117543, Singapore
E-mail: chmyaosq@nus.edu,sg
Prof. Dr. W. Huang
Shaanxi Institute of Flexible Electronics (SIFE) & Institute of Biomedical Materials & Engineering (IBME), Northwestern Polytechnical University (NPU), 127 West Youyi Road, Xi'an 710072, P. R. China
E-mail: iamwhuang@nwpu.edu.cn
Supporting information and the ORCID identification number(s) for the author(s) of this article can be found under https://doi.org/10.1002/anie.xxxxxxxxx

10.1002/anie.202000059

WILEY-VCH

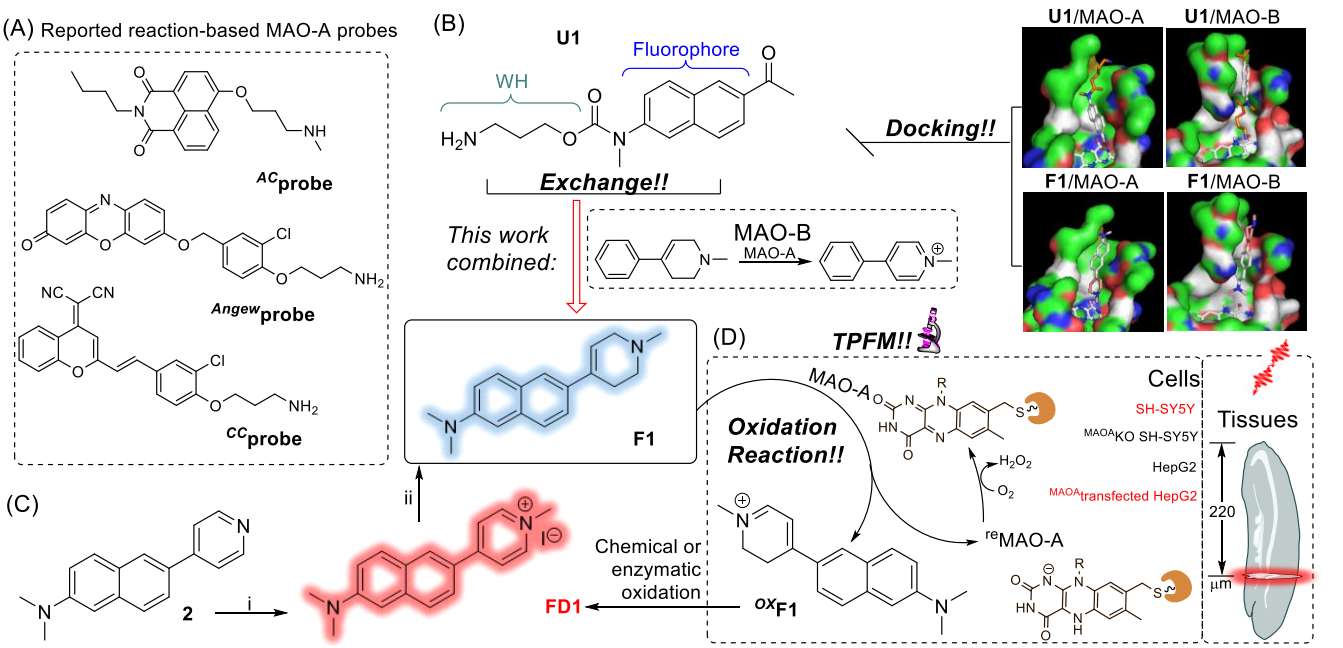

Figure 1. (A) Molecular structures of reported reaction-based MAO-A-specific OPFPs.[10] (B) The design principle of **F1** and docking results of **F1** and **U1** to the MAO-A and -B, respectively. The binding mode of **F1**/**U1** to MAO-A and -B at flavin-containing "substrate" cavity was viewed as a colorful solid. Both ligands and the redox-active isoalloxazine ring of flavin were shown in stick form for clarity. See Figure S1 in the Supporting Information for details. (C) The synthetic scheme of **FD1** and **F1**; i) CH_3I, MeCN, room temperature, 24 h; ii) $NaBH_4$, MeOH, 0 °C, 10 min. For details, see Supporting Information. (D) Overall strategy for visualizing MAO-A-specific activity with **F1** in live mammalian cells and tissues by using TPFM; ^{ox}**F1** is the oxidized form of **F1**, ^{MAOA}KO SH-SY5Y denotes the MAO-A knockout SH-SY5Y cells, ^{MAO}transfected HepG2 denotes MAO-A-overexpressed HepG2 cell lines, ^{re}MAO-A denotes the reduced form of MAO-A.

to have projected closer toward FAD, with a measured distance of 3.5 Å between the pyridine nitrogen in **F1** and C5 in FAD (Figure 1B, right bottom and Figure S1). In the docked **F1**/MAO-B structure on the other hand, the *N*,*N*-dimethyl group has oriented towards FAD, making **F1** unsuitable as a MAO-B substrate. On the basis of above design principle, the MAO-A-specific TPFP **F1**, as well as **FD1** (**F1**-oxidized product, in red halo), was successfully synthesized and fully characterized (Figure 1C and Supporting Information). The expected MAO-A-dependent two-photon fluorescence Turn-ON strategy of **F1** is shown in Figure 1D; the initially non-fluorescent **F1** would first undergo MAO-A-catalyzed oxidization to ^{ox}**F1**, followed by rapid conversion to **FD1** (*via* chemical/enzymatic oxidation in the system[12a]). The introduction of pyridinium (a strong electron-withdrawing moiety with good conjugation) in **FD1** would result in the formation of a push-pull

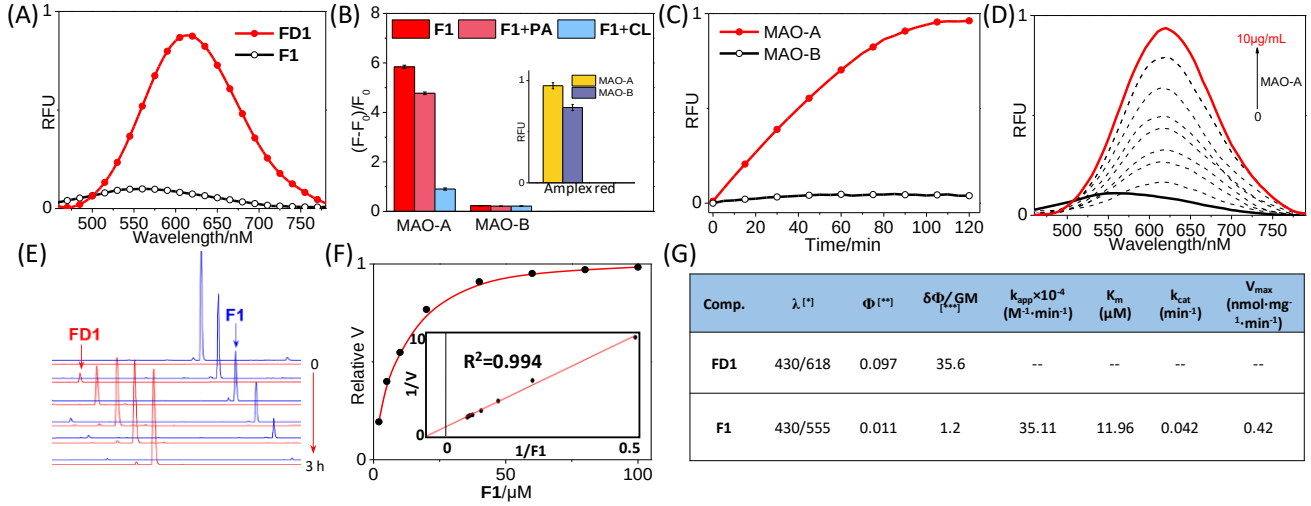

(G)

Comp.	λ [*]	Φ [**]	δΦ/GM [***]	k_{app}×10^{-4} (M^{-1}·min^{-1})	K_m (μM)	k_{cat} (min^{-1})	V_{max} (nmol·mg^{-1}·min^{-1})
FD1	430/618	0.097	35.6	--	--	--	--
F1	430/555	0.011	1.2	35.11	11.96	0.042	0.42

Figure 2. (A) One-photon excited fluorescence spectra with 1.0 μM of **F1** and **FD1** in PBS buffer. (B) Fluorescence changes of **F1** (1.0 μM) in MAO-A or -B (10 μg mL^{-1}; in PBS buffer) at 37 °C upon 2-h incubation, with or w/o an inhibitor (1 μM) where indicated. (Inset): RFU of enzyme/Amplex Red Kit upon 1-h incubation with the enzyme. Full spectra are shown in Figure S3. (C) Time-dependent (0-120 min) fluorescence intensity profiles of **F1** (1.0 μM) upon incubation with MAO-A or -B (10 μg mL^{-1}), respectively. (D) Fluorescence spectra of **F1** (1.0 μM) upon 2-h incubation with various concentrations of MAO-A in PBS buffer at 37 °C. (E) HPLC profiles of MAO-A (10 μg mL^{-1})-catalyzed oxidation of **F1** (1.0 μM) to **FD1**. Reactions were carried out at 37 °C in PBS buffer and monitored by analytical HPLC-MS (equipped with a fluorescence detector) from 0 to 3 h ($\lambda_{ex/em}$ = 310/450 and 430/620 nm for **F1** and **FD1**, respectively). Peaks were unambiguously assigned based on their molecular weights. (F) Kinetic studies of (**F1** + MAO-A) enzymatic reaction over a **F1**-concentration range (0-100 μM) with MAO-A (10 μg mL^{-1}) in PBS buffer at 37 °C. (Inset): fitted Linewearver-Burk plot. (G) The corresponding photophysical properties and kinetic data of **F1** and **FD1**; [*] peak position of the emission band; [**] one-photon fluorescence quantum yield (Φ) upon the absorption maximum of **FD1**, using coumarin-6 (Φ = 0.85) as a reference for measurement; [***] the maxima two-photon action cross section values upon excitation wavelength of fluorophore from 750 to 840 nm in GM (1 GM = 10^{-50} cm^4 s $photon^{-1}$); --: not determined. $\lambda_{ex/em}$ = 430/620 nm; PBS buffer (*p*H 7.4) supplemented with 0.4% Triton X-100.

10.1002/anie.202000059

WILEY-VCH

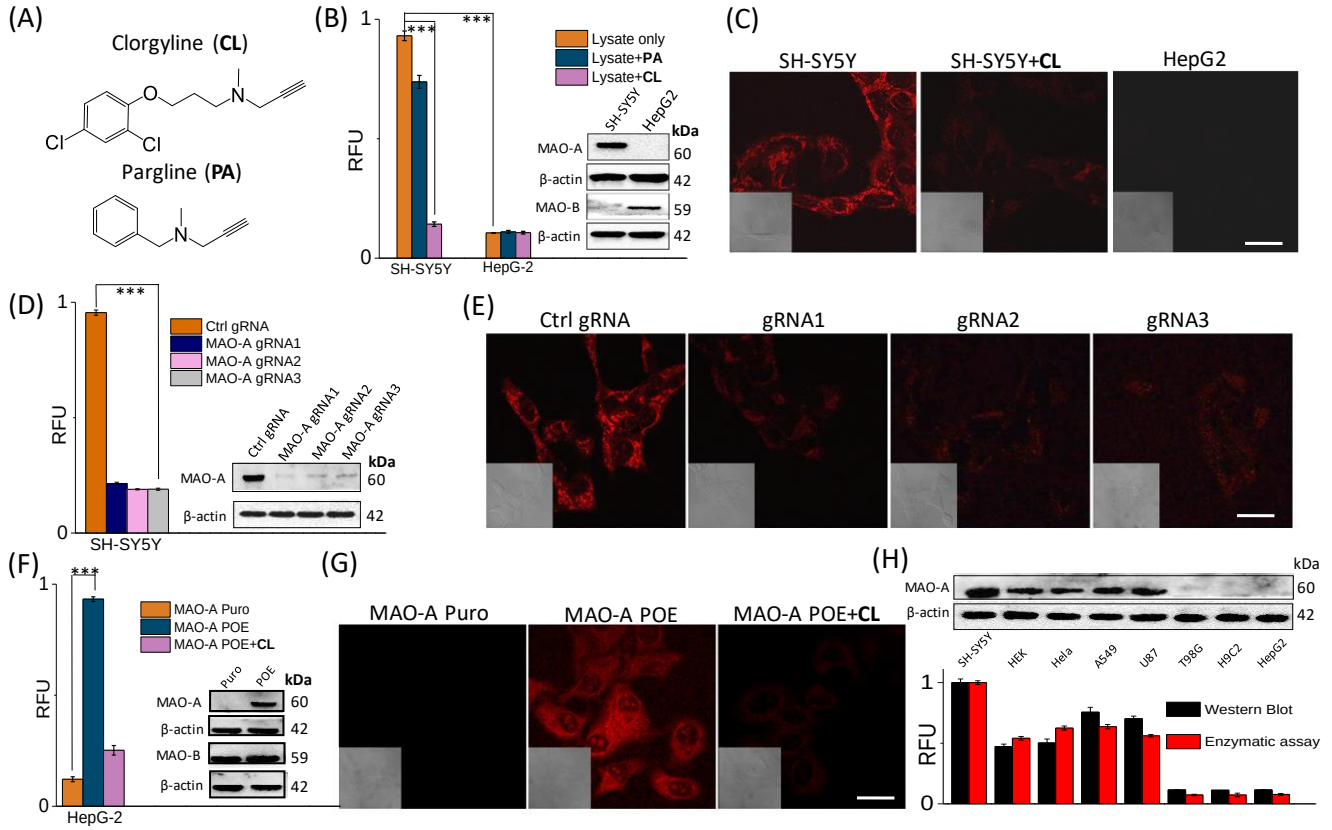

Figure 3. Fluorescence detection and bioimaging of MAO-A activity by **F1** in live mammalian cells. (A) Structure of irreversible MAO-A-selective inhibitor clorgyline (**CL**) and MAO-B-selective inhibitor pargyline (**PA**). (B) Fluorescence changes of **F1** (1.0 μM) in SH-SY5Y lysates (500 μg mL^{-1}) in assay buffer with or w/o an inhibitor (10 μM **CL**/**PA**), where indicated; HepG2 cell lysates were used as negative controls. (C) One-photon confocal fluorescence images of live SH-SY5Y (with or w/o 1-h pretreatment of 50 μM **CL**) incubated with **F1** (10 μM) for 2 h. **F1**-treated HepG2 cells were used as negative controls. (D) RFU of **F1** (1.0 μM) + lysates (500 μg mL^{-1}) in assay buffer from MAO-A-knocked down SH-SY5Y cells. (Inset): corresponding WB results of the lysates. Cells treated with different gRNA (Ctrl & gRNA/1/2/3) were used. (E) One-photon confocal fluorescence images of live MAO-A-knocked down SH-SY5Y cells upon incubation with **F1** (10 μM) for 2 h. (F) RFU of **F1** (1.0 μM) + lysates (500 μg mL^{-1}) in assay buffer with MAO-A-expressing HepG2 cells, with inhibitor (10 μM **CL**) where indicated. (Inset): corresponding WB results of the lysates. Cells treated with Puro and POE (negative control) were used. (G) One-photon confocal fluorescence images of live MAO-A-expressing HepG2 cells (with 1-h pretreatment of 50 μM **CL** where indicated) upon incubation with **F1** (10 μM) for 2 h. (H) RFU calculated from the fluorescence assay of proteome lysates from eight different mammalian cell lines upon incubation with **F1** (in red). For comparison, the relative WB signals of endogenous MAO-A expression from the same cells were quantified and plotted (in black). The WB results are shown (on top). Error bars represent standard error of the mean (s.e.m). (n = 3), the linear regression fitting data is shown in Figure S12. ***P < 0.001, n = 3, Student's t-test, two-tailed in (B/D/F). Differential interference contrast (DIC) images of related confocal fluorescence images for (C/E/G) are shown in the bottom-left of the corresponding image panels; scale bar = 25 μm.

system around the naphthalene fluorophore, thus ensuring **F1**-to-**FD1** conversion to be highly fluorogenic (that is, Turned-ON) and detectable by TPFM.[8a] The subsequent evaluation of **F1** against a variety of biological samples, including recombinant MAO proteins, mammalian cell lysates, live mammalian cells, and mouse brain/tumor tissues, with both *in vitro* fluorescence-based enzymatic assay and one/two-photon fluorescence imaging, indicated that **F1** was indeed highly selective towards MAO-A even at high MAO-B expression levels, as shown in Figures 2/3/4.

First, we evaluated the photophysical properties of **F1** and **FD1** under physiological conditions (PBS buffer supplemented with 0.4% Triton X-100, *p*H 7.4). As shown in Figure S2, **F1** and **FD1** had absorption/emission maxima at 305/450 nm and 430/620 nm, respectively. Upon excitation at 430 nm (maximum absorption wavelength of the fluorophore), **FD1** exhibited a strong red fluorescence which peaked at ~620 nm, with a one-photon fluorescence quantum yield of 0.097 and a two-photon action cross section of 35.6 (Figure 2A/G). Meanwhile, the fluorescence signal of **F1** was very weak at 555 nm, with a lower one-photon fluorescence quantum yield of 0.011 and a two-photon action cross section of ~1.2. Such properties thus made the **F1**-to-**FD1** conversion system and therefore **F1** a suitable fluorogenic probe for two-photon excited (~800 nm) fluorescence imaging in deep tissues.[8] Next, we assessed the enzymatic activity of **F1** with both recombinant human MAOs, and unequivocally confirmed that **F1** was exclusively MAO-A-responsive (Figure 2B-G). The *in vitro* assay was carried out concurrently with **F1** (1.0 μM; in PBS buffer, *p*H 7.4) and the corresponding enzyme (10 μg mL^{-1}) at 37 °C, and fluorescence measurement was recorded after 2 h. The commercially available Amplex Red MAO Assay kit was used as a reference to normalize the relative MAO-A/B activity under similar conditions (Figure 2B, inset);[9a,10] both enzymes produced significant increases in fluorescence, with MAO-A showing a slightly higher activity than that of MAO-B. In sharp contrast, significant increases in **F1** fluorescence were detected ONLY in MAO-A (i.e. **F1** + MAO-A) but not MAO-B (i.e. **F1** + MAO-B) enzymatic reactions under identical conditions, and they were nearly completely abolished in the presence of a MAO-A specific inhibitor, **CL** (i.e. **F1** + **CL** + MAO-A). Addition of a MAO-B specific inhibitor, **PA**, to the same reaction (i.e. **F1** + MAO-A + **PA**) only caused a slight suppression in **F1** fluorescence increase. Concurrently, time-dependent fluorescence measurements were carried out for both enzymatic reactions (i.e. **F1** + MAO-A and **F1** + MAO-B; Figure 2C); a concomitant fluorescence increase was observed in the former, but not in the latter, and the resulting sigmoidal curve could be used to provide the corresponding reaction constant of k_{app} = 35.11 × 10^4 M^{-1} min^{-1} for (**F1** + MAO-A) reaction (summarized in Figure 2G). We next carried out concentration-dependent reactions for both enzymatic reactions (Figures 2D & S4); for assays carried out at 0-10 μg mL^{-1} enzyme concentrations and 2-h incubation time, only the (**F1** + MAO-A) reactions produced significant fluorescence increases (Figure 2D).

10.1002/anie.202000059

WILEY-VCH

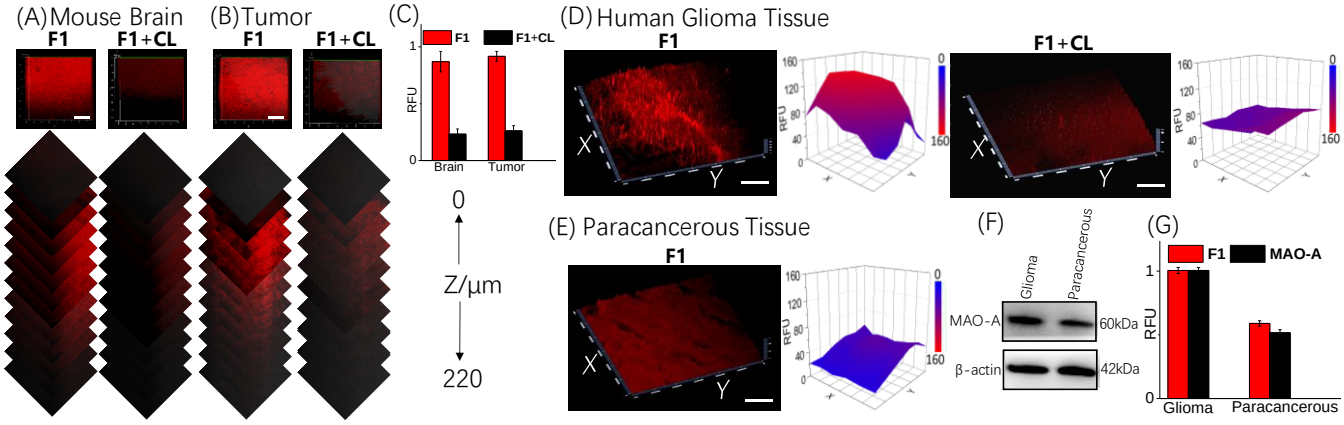

Figure 4. TPFM imaging of endogenous MAO-A activity with **F1**-treated (50 μM, 3 h) fresh mice brain (A) and SH-SY5Y tumor slices (B). **CL**-pretreatment (200 μM, 1 h) was done where indicated. Images were scanned once every 20 μm for a total depth of 220 μm; scale bar = 100 μm. (C) Average fluorescence intensity profiles of reconstructed tissues image in (A/B). (D) TPFM images and the correspnding quantified plots (right) of **F1**-treated (50 μM, 3 h) fresh human glioma tissue (50 μm depth). Results from the corresponding **CL**-pretreated (200 μM, 1 h) samples were shown. (E) TPFM image (left) and the corresponding quantified plot (right) of **F1**-treated (50 μM, 3 h) fresh paracancerous tissue slices (50 μm depth). scale bar = 100 μm. (F) WB results for (D/E). (G) Comparison of average fluorescence intensity profiles of images from (D/E; red bars) and relative endogenous MAO-A expression levels determined by the WB results from (F; black bars) of the tissues; error bars represent standard error of the mean (s.e.m). (n = 3).

No obvious fluorescence increase was observed in the (**F1** + MAO-B) reaction (Figure S4). The reaction parameters were further optimized under physiological conditions (*p*H 7.4 and 37 °C, see Figure S5). Next, by using analytical HPLC-MS equiped with a fluorescence detector, we unequivocally confirmed the successful **F1**-to-**FD1** conversion catalyzed by MAO-A, presumably through the formation of the highly unstable ^{ox}**F1** intermediate (not observed in HPLC; Figure 2E). We also studied the selectivity of the (**F1** + MAO-A) reaction with a variety of potential interfering species (Figure S6); **F1** showed a high selectivity toward MAO-A over all other species tested, which was attributed to the specific oxidation reaction of this fluorogenic substrate catalyzed exclusively by MAO-A. Finally, we performed a detailed kinetic study on the (**F1** + MAO-A) reaction and obtained the corresponding Michaelis-Menten constants (K_m = 11.96 μM, k_{cat} = 0.042 min^{-1}, V_{max} = 0.42 nmol·mg^{-1}·min^{-1}; Figure 2F/G). Of note, the K_m value of **F1** was similar to those of previously reported MAO-A-specific OPFPs.[10] As the (**F1** + MAO-B) reaction produced a negligible increase in fluorescence under all tested conditions, we were unable to obtain its kinetic data. We thus concluded that **F1** was indeed a fluorogenic probe suitable for the sensitive and continuous reporting of MAO-A activity with minimal cross-activity towards MAO-B, and, with its excellent two-photon fluorescence properties (that is, upon enzymatic conversion to **FD1**), might serve as a good MAO-A-specific TPFPs in various biological applications.

Encouraged by above results, we next determined whether **F1** could be used to specifically detect MAO-A activities in complex biological samples. Human-derived SH-SY5Y and HepG2 cells are two disease cell lines known to express elevated levels of MAO-A and -B activities, respectively.[13] We first confirmed the over-expressed MAO-A, but not MAO-B, activity in SH-SY5Y cell lysates by directly incubating them with **F1** in the presence of **CL** or **PA** (Figure 3A/B); results showed that the (**F1** + SH-SY5Y) reaction produced significant levels of **CL**-sensitive fluorescence signals, which were attributed to the endogenous MAO-A activity and subsequently confirmed by Western blotting (WB) analysis of the cell lysates (inset of Figure 3B). On the other hand, (**F1** + HepG2) reaction failed to generate any above-background fluorescence under similar conditions, and the WB results with the corresponding lysates also confirmed the expected endogenous expression of MAO-B but not MAO-A activity. Concurrently, real-time fluorescence bioimaging was used to test the capability of **F1** for visualizing MAO-A activity in live cells. We first established that **F1** was minimally cytotoxic to most mammalian cells at concentrations up to 50 μM (12-h incubation; Figure S7). Subsequent live-cell imaging of **F1**-treated SH-SY5Y cells by using fluorescence microscopy demonstrated a progressive increase in **CL**-sensitive fluorescence signals (Figures 3C & S8/9), but not in live HepG2 cells. Meanwhile, **F1**-treated SH-SY5Y lysates/live cells (pretreated with different concentrations of **CL** from 0 to 50 μM) showed dose-dependent fluorescence decreases (Figure S10/11). To further validate the MAO-A selectivity of **F1**, endogenous MAO-A-knocked-down SH-SY5Y and stably MAO-A-overexpressed HepG2 cells were created (Figure 3D and 3F, respectively); as shown in the WB results of Figure 3D (inset), by using the corresponding lentiviral Crispr/Cas9 system (gRNA1/2/3, with Ctrl gRNA as a non-targeting gRNA vector control), we obtained live SH-SY5Y cells in which endogenous MAO-A was successfully knocked down.As shown in Figure 3E, in the absence of endogenous MAO-A expression, the corresponding **F1**-treated SH-SY5Y cells failed to generate detectable fluorescence signals. In contrast, with MAO-A-expressing HepG2 cells treated with **F1** (Figure 3F; POE, with Puro as an empty vector control; see Supporting Information for details),[14] we observed MAO-A enzymatic activity in both the proteome lysates and live cells (Figure 3F/G); a significant level of **CL**-sensitive fluorescence signals were detected. Finally, we incubated **F1** with eight different mammalian cell lines (SH-SY5Y, HEK293, U87, T98G, HeLa, A549, H9C2 and HepG2). Fluorescence readings and endogenous MAO-A expression levels (based on WB results; Figure 3H, top) were measured; there was a good correlation between the two sets of fluorescence values (Figures 3H, bottom & S12). Unlike the general MAO assays that require a physical separation of the MAO-A protein, **F1** provides a simple, rapid and selective method for reporting endogenous MAO-A activities directly from crude cell proteomes and live mammalian cells alike.

Inspired by our success in cell-based experiments, we next determined whether **F1** could be used to image MAO-A activities from deep tissues (e.g. muse/human brain and tumor tissues) by using TPFM. Neurons and glial cells were previously reported to have elevated expression levels of MAO-A.[15] We first confirmed minimal cytoxicity of MPTP, MPP$^+$, **F1**, and **FD1** in two well-known neuronal cells, PC12 and SH-SY5Y (Figure S13/S14); no toxicity was observed in both cell lines with up to 50 μM of probe treatment. We next injected **F1** and MPTP intraperitoneally into two groups of mice, after which one group underwent behavioral observation, while the other group underwent H&E staining of brain tissues after 2 h (Figures S14/S15); our results indicate there was no significant apoptosis of the substantia nigral cells in **F1**-

injected mice (Figure S15), and their motor performance was not significantly affected either (Figure S16 & Supplementary Video).[16] These findings thus showed that **F1** did not possess significant cellular or biological toxicities at the assay/imaging concentrations. In the two-photon fluorescence imaging results (Figures 4A/B/C & S17), we detected similar **CL**-sensitive fluorescence signals in both **F1**-treated fresh tissue slices isolated from brains of normal mice and those transplanted with tumors. Finally, we detected strong **CL**-sensitive fluorescence signals in **F1**-treated fresh human glioma tissues which corroborated well with the corresponding endogenous MAO-A expression level from WB results (Figure 4D/F), whereas in **F1**-treated paracancerous tissue slices (negative controls), comparatively weaker fluorescence signals were detected, consistent with their relatively low MAO-A expression in such tissues (Figures 4E/F/G & S19).

In summary, we have successfully developed a TPFP (**F1**) with excellent specificity for detecting/visualizing MAO-A activities from various biological samples by using one- and two-photon fluorescence spectroscopy. The two-photon performance of **F1** enabled it to sensitively and selectivevly image MAO-A activities from fresh mouse/human brain and tumor tissues. Importantly, our results demonstrated the feasibility of using SMFPs to explore the chemistry and biology of MAO-A at the organism level, thus providing a useful chemical tool for future studies of MAO-A-related diseases like glioma.

Acknowledgements

This work was financially supported by the National Natural Science Foundation of China (81672508, 81773802, 81671910), Jiangsu Provincial Foundation for Distinguished Young Scholars (BK20170041), Natural Science Foundation of Shaanxi Province (2019JM-016, 2019KJXX-089), China-Sweden Joint Mobility Project (51811530018), Fundamental Research Funds for the Central Universities, GSK-EDB Trust Fund (R-143-000-688-592), and the Synthetic Biology Research & Development Programme (SBP) of the National Research Foundation (SBP-P4 and SBP-P8), Singapore.

Conflict of interest

The authors declare no conflict of interest.

Keywords: monoamine oxidase A · MPTP · two-photon fluorogenic probes · bioimaging · glioma

[1] a) J. C. Shih, K. Chen, M. J. Ridd, *Annu. Rev. Neurosci.* **1999**, *22*, 197-217; b) R. J. Nelson, B. Trainor, *Nat. Rev. Neurosci.* **2007**, *8*, 536-546.

[2] a) K. Westlund, R. Denney, L. Kochersperger, R. Rose, C. W. Abell, *Science* **1985**, *230*, 181-183; b) J. P. Finberg, J. M. Rabey, Front Pharmacol. **2016**, *7*, 340.

[3] a) J. C. Shih, R. F. Thompson, *Am. J. Hum. Genet.* **1999,** *65*, 593-598; b) C. M. B. Pare, C. N. Hallstrom, *Lancet* **1982**, *2*, 183-186.

[4] a) X. M. Ou, K. Chen, J. C. Shih, *Proc. Natl. Acad. Sci. USA.* **2006**, *103*, 10923-10928; b) H. G. Brunner, M. Nelen, X. O. Breakefield, *Science* **1993**, *262*, 578-580; c) J. S. Fowler, N. D. Volkow, G. J. Wang, *Nature* **1996**, *379*, 733-736.

[5] R. McDermott, D. Tingley, J. Cowden, *Proc. Natl. Acad. Sci. USA* **2009**, *106*, 2118-2123.

[6] a) M. B. H. Youdim, D. Edmondson, K. F. Tipton, *Nat. Rev. Neurosci.* **2006**, *7*, 295-309; b) R. Mcdermott, D. Tingley, J. Cowden, G. Frazzetto, D. D. P. Johnson, *Proc. Natl. Acad. Sci. USA* **2009**, *106*, 2118-2123; c) R. Shi, Q. Wu, C. Xin, H. Yu, K. Lim, X. Li, Z. Shi, C. Zhang, L. Qian, L. Li, W. Huang, *ChemBiochem*, **2019**, *20*, 1487-1497.

[7] a) H. M. Kim, B. R. Cho, *Chem. Rev.* **2015**, *115*, 5014-5055; b) H. Zhu, J. Fan, J. Du, X. Peng, *Acc. Chem. Res.* **2016**, *49*, 2115-2126; c) J. Chan, S. C. Dodani, C. J. Chang, *Nat. Chem.* **2012**, *4*, 973-984; d) J. Zhang, X. Chai, X. P. He, H. J. Kim, J. Yoon, H. Tian, *Chem. Soc. Rev.* **2019**, *48*, 683-722; e) D. Kim, Y. W. Jun, K. H. Ahn, *Bull. Korean Chem. Soc.* **2014**, *35*, 1269-1274.

[8] a) L. Qian, L. Li, S. Q. Yao, *Acc. Chem. Res.* **2016**, *49*, 626-634; b) A. Song, A. S. Charles, S. A. Koay, J. L. Gauthier, S. Y. Thiberge, J. W. Pillow, D. W. Tank, *Nat. Methods.* **2017**, *14*, 420-426; c) T. B. Ren, W. Xu, Q. L. Zhang, X. X. Zhang, S. Y. Wen, H. B. Yi, L. Yuan, X. B. Zhang, *Angew. Chem. Int. Ed.* **2018**, *57*, 7473-7477; *Angew. Chem.* **2018**, *130*, 7595-7599.

[9] a) L. Li, C. W. Zhang, C. Y. J. Chen, B. W. Zhu, C. Chai, Q. H. Xu, E. K. Tan, Q. Zhu, K. L. Lim, S. Q. Yao, *Nat. Commun.* **2014**, *5*, 3176; b) D. Kim, S. H. Baik, S. Kang, S. W. Cho, J. Bae, M. Y. Cha, M. J. Sailor, I. Mook-Jung, K. H. Ahn, *ACS Cent. Sci.* **2016**, *2*, 967-975; c) D. Kim, S. Sambasivan, H. Nam, K. H. Kim, J. Y. Kim, T. Joo, K. H. Lee, K. T. Kim, K. H. Ahn, *Chem. Commun.* **2012**, *48*, 6833-6835.

[10] a) X. Wu, W. Shi, X. Li, H. Ma, *Angew. Chem. Int. Ed.* **2017**, *56*, 15319-15323; *Angew. Chem.* **2017**, *129*, 15521-15525; b) X. Wu, L. Li, W. Shi, Q. Gong, X. Li, H. Ma, *Anal. Chem.* **2016**, *88*, 1440-1446; c) Z. Yang, W. Li, H. Chen, Q. Mo, J. Li, S. Zhao, C. Hou, J. Qin, G. Su, *Chem. Commun.* **2019**, *55*, 2477-2480; d) W. Shen, J. Yu, J. Ge, R. Zhang, F. Cheng, X. Li, Y. Fan, S. Yu, B. Liu, Q. Zhu, *ACS Appl. Mater. Interfaces.* **2016**, *8*, 927-935.

[11] K. Cakir, S. S. Erdem, V. E. Atalay. *Org. Biomol. Chem.* **2016**, *14*, 9239-9252.

[12] a) Herraiz T, *J Enzyme Inhib. Med. Chem.* **2012**, *27*, 810-817; b) A. J. Trevor, T. P. Singer, R. R. Ramsay, Jr. N. Castagnoli, *J Neural. Transm. Suppl.* **1987**, *23*, 73-89; c) S. Long, L. Chen, Y. Xiang, M. Song, Y. Zheng, Q. Zhu, *Chem. Commun.* **2012**, *48*, 7164-7166.

[13] a) J. C. Shih, K. Chen, *Curr. Med. Chem.* **2004**, *11*, 1995-2005; b) M. Naoi, W. Maruyama, Y. Akao, H. Yi, Y. Yamaoka, *J. Neural. Transm. Suppl.* **2006**, *71*, 67-77.

[14] a) F. Zhang, Hum. Gene Ther. **2015**, *26*, 409-410; b) M. R. Ahmed, A. Berthet, E. Bychkov, G. Porras, Q. Li, B. H. Bioulac, Y. T. Carl, B. Bloch, S. Kook, I. Aubert, S. Dovero, E. Doudnikoff, V. V. Gurevich, E. V. Gurevich, E. Bezard, *Sci. Transl. Med.* **2010**, *2*, 28ra28.

[15] J. Tong, G. Rathitharan, J. H. Meyer, Y. Furukawa, L. C. Ang, I. Boileau, M. Guttman, O. Hornykiewicz, S. J. Kish, *Brain* **2017**, *140*, 2460-2474.

[16] a) T. Archer, A. Fredriksson, *Neurotox. Res.* 2013, 24, 393-406; b) M. Sedelis, R. K. Schwarting, J. P. Huston, *Behav. Brain Res.* **2001**, *125*, 109-125.

10.1002/anie.202000059

WILEY-VCH

Table of Contents

COMMUNICATION

Text for Table of Contents

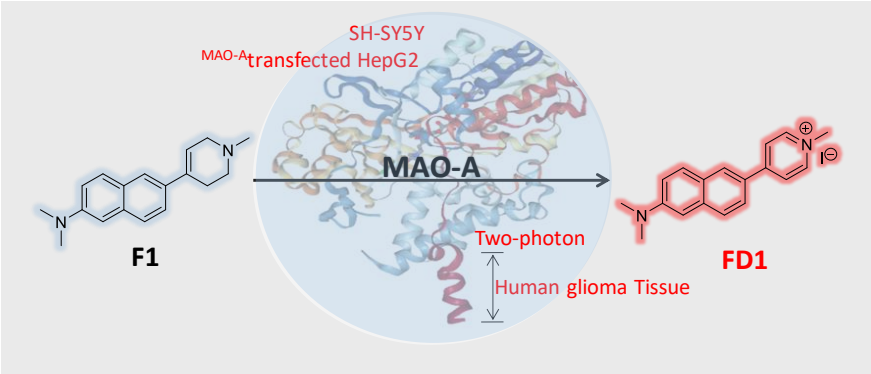

Picking MAO-A: By using two-photon fluorescence microscopy, a novel two-photon fluorogenic probe (**F1**) is shown to successfully detect endogenous MAO-A activities from a variety of biological samples, including live mammalian cells, fresh mouse/human brain and tumor tissues, with minimal cytotoxicity and cross-reactivity toward MAO-B.

H. Fang, H. Zhang, L. Li, Y. Ni, R. Shi, Z. Li, X. Yang, B. Ma, C. Zhang, Q. Wu, C. Yu, N. Yang, S. Q. Yao* and W. Huang**

Page No. – Page No.

Rational Design of Two-photon Fluorogenic Probe for Visualizing Monoamine Oxidase A Activity in Human Glioma Tissues